A unique strategy towards high dielectric constant and low loss with multiwall carbon nanotubes anchored onto graphene oxide sheets

Sourav Biswas,[†] Goutam Prasanna Kar,[†] Deepshikha Arora and Suryasarathi Bose*

Multiwall carbon nanotubes (MWNTs) were anchored onto graphene oxide sheets (GOs) *via* diazonium and C–C coupling reactions and characterized by spectroscopic and electron microscopic techniques. The thus synthesized MWNT–GO hybrid was then melt mixed with 50/50 polyamide6–maleic anhydride-modified acrylonitrile-butadiene-styrene (PA6–mABS) blend to design materials with high dielectric constant (ε') and low dielectric loss. The phase morphology was studied by SEM and it was observed that the MWNT–GO hybrid was selectively localized in the PA6 phase of the blend. The ε' scales with the concentration of MWNT–GO in the blends, which interestingly showed a very low dielectric loss (<0.2) making them potential candidate for capacitors. In addition, the dynamic storage modulus scales with the fraction of MWNT–GO in the blends, demonstrating their reinforcing capability as well.

Introduction

Polymeric composites with high dielectric constant and low dielectric loss have received considerable attention in the recent past.[1–4] They have been explored for various applications in high energy storage devices, electronics and other industries.[5–7] Dielectric properties arise from the uneven displacement of electrons under an external electric field. Complex permittivity is expressed as $\varepsilon^* = \varepsilon' - i\varepsilon''$, where ε' and ε'' are the real and imaginary parts of the complex permittivity.[8–10] According to the Kramers–Kronig relation, ε' and ε'' depend on the frequency, ω, of the applied electric field, and this is expressed as Kramers–Kronig relation,[11]

$$\varepsilon'(\omega) = \varepsilon_0 + \frac{2}{\pi} \int_0^\infty \frac{u\varepsilon''(u)}{u^2 - \omega^2} du \qquad (1)$$

The real part of the permittivity is expressed as $\varepsilon' = \varepsilon_0 \varepsilon_r$, where ε_0 is the vacuum permittivity (8.85×10^{-12} F m^{-1}) and ε_r is the relative permittivity of the material. Higher values of ε' indicate the material's ability to store energy under an applied electrical field. The imaginary part of the permittivity (ε'') is the dielectric loss. It is envisaged that under the influence of an external electric field, part of the electrical energy is dissipated as heat due to charge hopping. Hence, for better performance, this dielectric loss needs to be

minimized. The energy stored by a parallel plate capacitor is given by

$$W = \frac{1}{2} C V_{br}^2 \qquad (2)$$

where V_{br} is the breakdown voltage and C is the capacitance, given by

$$C = \varepsilon_0 \varepsilon_r \frac{A}{l} \qquad (3)$$

A is the area and l is thickness of the parallel plate capacitor. Hence, the volumetric energy density is given by

$$W' = \frac{1}{2} \varepsilon_0 \varepsilon_r E_{br}^2 \qquad (4)$$

where $E_{br} = \frac{V_{br}}{l}$ is the breakdown field strength.

Polymers generally have a very low dielectric constant (<10) but high breakdown field strength.[6] On the other hand, ferroelectric ceramic particles have a very high dielectric constant (ε') but very low breakdown strength.[12] So, a high ε' and low loss can be achieved by incorporating ceramic particles into a polymer matrix. But this strategy usually requires a higher fraction of the ceramic particles and hence produces an unwanted increase of the composite rigidity.[13] In most other cases the increase of the dielectric constant has been met with relatively high loss tangent values, which is also an important factor while considering materials for capacitor applications.[14] Due to the addition of ferroelectric ceramic particles, the interfacial polarization is increased.[12] Hence, it is very difficult to obtain high dielectric permittivity and low loss tangent values at the same time. However, by altering the interfacial interaction

Department of Materials Engineering, Indian Institute of Science, Bangalore-560012, India. E-mail: sbose@materials.iisc.ernet.in; Tel: +91-80-2293 3407

† GPK and SB made equal contribution to this work.

between the ceramic particles and the polymer matrix, the dielectric constant can be tuned.[5] So, the surface chemistry of the particles can play an important role in obtaining materials with a high dielectric constant.[15,16]

In the recent past, in view of good electrical and mechanical integrity, carbon-based nanostructures like multiwall carbon nanotubes (MWNTs) and graphene have attracted a great deal of interest for a wide range of applications.[17,18] MWNTs show relatively high dielectric loss due to energy dissipation.[8] Recently, reduced graphene oxide sheets (rGO) with partial chlorination were shown to exhibit a high dielectric constant and low dielectric loss, due to the polarizable C–Cl bond.[19]

In an attempt to enhance the dielectric constant and reduce the losses, a unique strategy was adopted here by chemically conjugating MWNTs with graphene oxide sheets. The hybrid nanoparticles were then melt blended with 50/50 (wt/wt) PA6–mABS blends, which have a low dielectric constant but are mechanically stable. The dielectric, rheological and dynamical mechanical properties were evaluated as a function of the amount of hybrid particles.

Experimental section

Materials

PA6 (1022B) was kindly provided by Ube Industries. mABS (Bondyram 6000, MFI 8 g per 10 min) was obtained from Polyram. The pristine MWNTs (NC 7000 of 90% purity, with an average diameter of 9.5 nm and an average length of 1.5 μm) were obtained from Nanocyl, Belgium. 4,4′-Methylenedianiline (MDA) was procured from Sigma Aldrich. The solvents like ethanol, tetrahydrofuran (THF), chloroform ($CHCl_3$), hydrochloric acid and sodium nitrite ($NaNO_2$) were obtained from Merck, India.

Synthesis of NH_2 terminated GO

GO was synthesized by a modified Hummers method as described in our earlier work.[20] GO–NH_2 was synthesized by a nucleophillic substitution reaction.[21] Typically, 250 mg of GO was suspended in 100 ml of THF and sonicated to exfoliate the sheets. The dispersed GO was then mixed with 250 mg of MDA and refluxed in a oil bath under a nitrogen atmosphere at 80 °C for 8 h. The solids thus obtained were separated by vacuum filtration, and re-dispersed in 100 ml of ethanol. This was again subjected to vacuum filtration. By repeating this purification cycle for about four times, the obtained solids were dried at 60 °C under vacuum for 24 h, thus yielding GO–NH_2.

Synthesis of hybrid MWNT–GO

A diazotization reaction was adopted to synthesize MWNT–GO hybrid structures.[22] Briefly, the required amount of GO–NH_2 was added to 40% HCl and bath sonicated. $NaNO_2$ was then added under ice-cold conditions (0–5 °C) with stirring. This step converts GO–NH_2 to a diazonium salt of GO. After 2 h of stirring, the pre-sonicated MWNTs (in dilute HCl) were then added under an inert atmosphere. N_2 escapes from the diazonium salt of GO and a MWNT–GO hybrid is formed *via* a C–C coupling reaction. The mixture was then washed by dilute HCl followed by water

and vacuum dried overnight. The same amounts of MWNTs and GO–NH_2 were used, thus yielding MWNT–GO (1 : 1).

Blend preparation

50/50 (wt/wt) blends of PA6–mABS were prepared with or without MWNT–GO by melt mixing using a Minilab II HAAKE extruder CTW5 (7 cc) at 260 °C with a rotational speed of 60 rpm for 20 min.[23] The mixing was performed under N_2 atmosphere to prevent oxidative degradation. The samples were pre-dried at 80 °C in a vacuum oven for 24 h prior to processing to remove traces of moisture.[24]

Characterizations

Fourier transform infrared (FTIR) spectroscopy was carried out using Perkin-Elmer GX in the range of 4000–400 cm^{-1} using a resolution of 4 cm^{-1} and KBr pellets.

Transmission Electron Microscopy (TEM) images were acquired using a Tecnai G2 F30 at 300 kV.

Morphological analysis for various blends was assessed by using scanning electron microscope on ESEM (environmental scanning electron microscope) at a 10 kV accelerating voltage. The extruded samples were cryofractured in liquid nitrogen. Then the mABS phase was selectively etched out by chloroform at room temperature.

The complex viscosity and storage modulus of the melt state for all the blends were measured by using a Discovery Hybrid Rheometer (DHR-3), TA-instruments, using a parallel plate geometry of a 25 mm diameter and 1 mm gap. The extrude strands were vacuum dried at 80 °C for 12 h before performing the rheological measurements. Experiments were carried out at a fixed temperature of 260 °C by varying the frequency from 0.1 to 100 rad s^{-1} at 1% strain rate under nitrogen atmosphere to prevent any degradation of the sample.

Dielectric measurements were performed on compression-molded disks using an Alpha-N Analyzer (Novocontrol, Hundsangen, Germany) in the broad frequency range of $100 \leq \omega \leq 10^6$ Hz.

Dynamic mechanical thermal analysis (DMTA) was done on a TA Instruments Q800 Dynamic Mechanical Analyzer on a compression-molded film.

Results and discussion

Synthesis and characterization of MWNT–GO hybrids

The MWNTs were grafted onto the GO sheets by a diazotization reaction as described in Scheme 1. Amine groups were introduced onto the GO sheets by reacting with MDA. The amine groups of MDA react with the epoxy groups of the GO. The terminal amine groups thus generated on GO–NH_2 were converted to diazonium salt ($–N_2^+Cl^-$) by reacting with $NaNO_2$ in the presence of dilute HCl at 0–5 °C. The mixture was then heated to 75 °C, followed by the addition of MWNTs to facilitate the C–C coupling reaction with GO. This is well supported by FT-IR (Fig. 1a) where C–N bond formation (1300 cm^{-1}) further supports the reaction between the MWNTs and GO. The broad peak in the range 3650–3250 cm^{-1} is the overlap of the O–H and
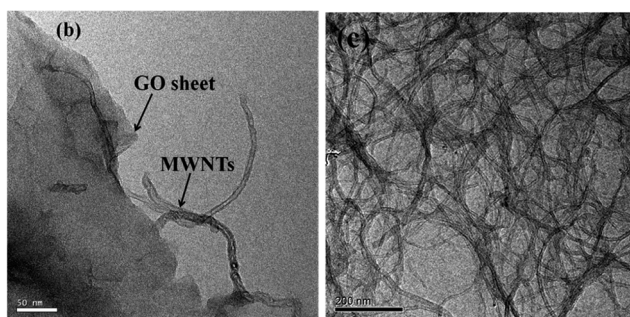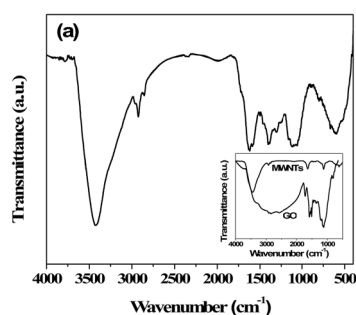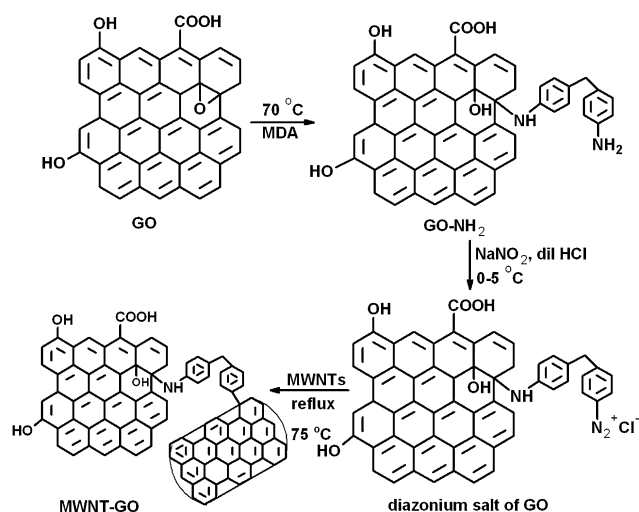
Scheme 1 Synthesis of MWNT–GO hybrid.

Fig. 1 (a) FT-IR spectra of MWNT–GO (inset shows the FTIR for GO–NH$_2$ and MWNTs) (b) TEM micrograph of MWNT–GO and (c) TEM micrograph of entangled MWNTs.

N–H vibrational frequencies.[21] The peak at 2930 cm^{-1} corresponds to the C–H stretching vibration. The HR-TEM images shown in Fig. 1b and c further confirm this conjugation between the MWNTs and GO sheets.

Phase morphology and selective localization of MWNT–GO in the blends

The phase morphology of PA6–mABS (50/50, wt/wt) blends with or without MWNT–GO hybrid was studied by SEM. The mABS phase was etched with chloroform.[25] The holes thus generated represent the etched out mABS phase as shown in Fig. 2.[26]
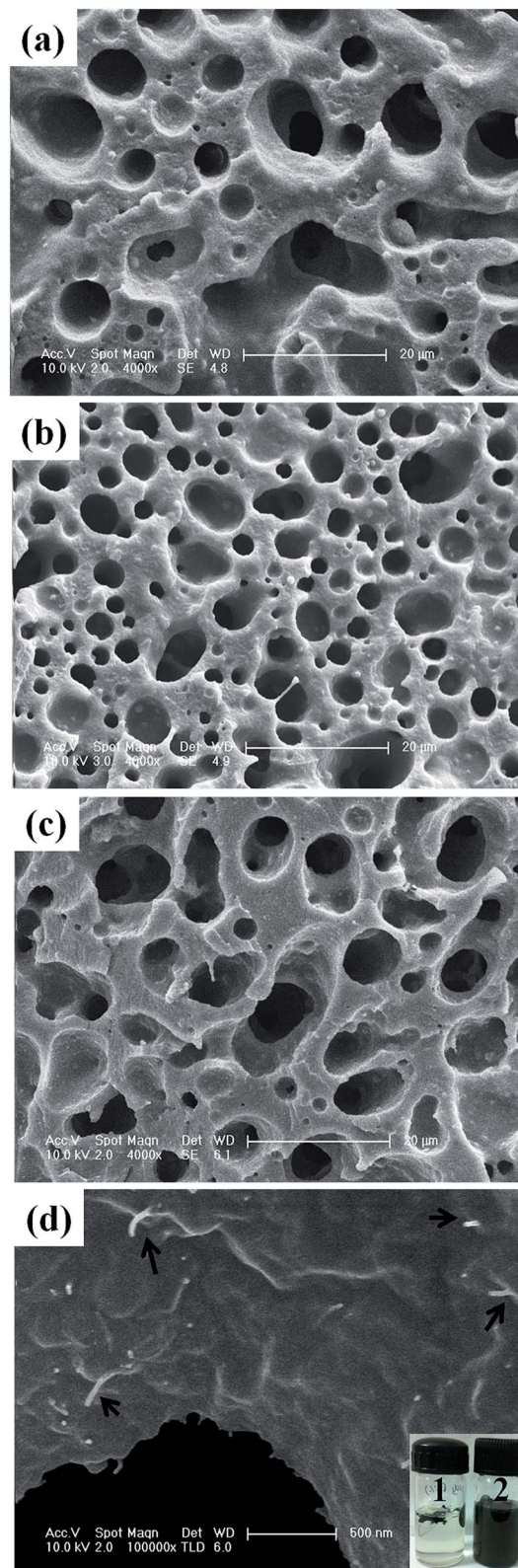

Fig. 2 SEM morphology of PA6–mABS (50/50, wt/wt) blends: (a) neat, (b) with 1 wt% MWNT– GO, (c) with 2 wt% MWNT–GO and (d) higher resolution images of (c) where the MWNTs are indicated as bright dots/tubes. (Inset showing the selective localization of the MWNT–GO hybrid in the PA6 phase. Vial 1 corresponds to PA6–mABS blends with 2 wt% MWNT–GO in CHCl$_3$ and vial 2 corresponds to PA6–mABS with 2 wt% MWNT–GO in formic acid.)

It is well known that PA6 and mABS are immiscible in nature, hence, they present a coarse morphology.[23] It is evident from Fig. 2 that mABS is randomly dispersed in the PA6 matrix. It is envisaged that the maleic anhydride groups in mABS can react with the PA6 during blending.[27] However, as the maleic anhydride content in mABS is less than 0.7 wt% (as provided by the supplier) the extent of the reaction can be less. The possibility of the terminal amine groups in PA6 reacting with the carbonyl acid groups of GO cannot be ruled out either. The possible reactions are explained in more detail in the next section by spectroscopic evidence. The SEM images (Fig. 2a–c) show a sea-island structure of the PA6–mABS blends in the presence of MWNT–GO.

The extent of various possible reactions was assessed by FT-IR (Fig. 3). The peaks at 2930 cm^{-1} for C–H stretching, 2236 cm^{-1} for C–N stretching, 1500–2000 cm^{-1} for polystyrene moieties and 1733 cm^{-1} for the C=O group of maleic anhydride are evident in the FTIR spectra of mABS.[25] The characteristic peak for free amine groups at 3292 cm^{-1} in the FTIR spectra for neat PA6 and the decrease in the intensity of this peak for the blends clearly suggest the reaction between the terminal amine groups in PA6 with either maleic anhydride groups in mABS or carbonyl groups on the GO. This is also supported by the peak at 3440 cm^{-1} corresponding to the hydrogen bonded amine group in the blends. In addition, the bands at 1633 cm^{-1} and 1539 cm^{-1} can be attributed to amide I and amide II, respectively, in the FTIR spectra for neat PA6. The bands at 1370, 1260 and 1205 cm^{-1} corresponding to amide III and CH$_2$ wagging are noted in the FTIR spectra for neat PA6.[25] In addition, the imide-five-ring deformation vibration appears at 749 cm^{-1}.

In order to assess the selective localization of the hybrid structure in the blends, solution-dissolution experiments were performed.[28] Typically, known amounts of the samples were dissolved in formic acid to remove the PA6 phase and in chloroform to remove the mABS phase from the blends. The vial containing formic acid turned dark after brief sonication indicating that the hybrid nanoparticles were selectively localized in the PA6 phase of the blend. This was further supported by the fact that the vial containing chloroform showed no change in colour. Moreover, the higher resolution SEM images show the nanoparticles in the remaining PA6 phase (Fig. 2d) where bright dots represent MWNTs.

State of dispersion assessed *via* melt rheology

Melt rheology is a very sensitive tool to study the state of dispersion of the nanoparticles in a given polymeric matrix.[21,29–32] Fig. 4a shows the storage modulus as a function of frequency for various blends. The storage modulus of PA6 is lower than mABS over the entire frequency range, while for the blends the storage modulus is in between that of the components. Blends with MWNT–GO hybrid particles exhibited a higher storage modulus with respect to the neat blends. In addition, the storage modulus scales with increasing fraction of MWNT–GO in the blends, indicating restricted motion of the macromolecules in the flow field.
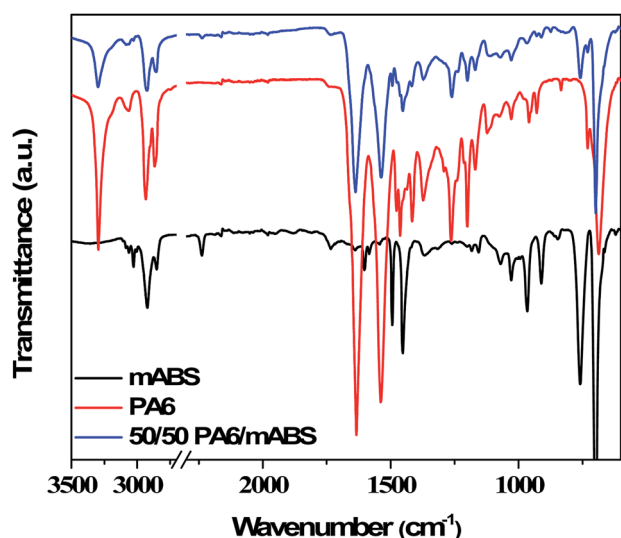

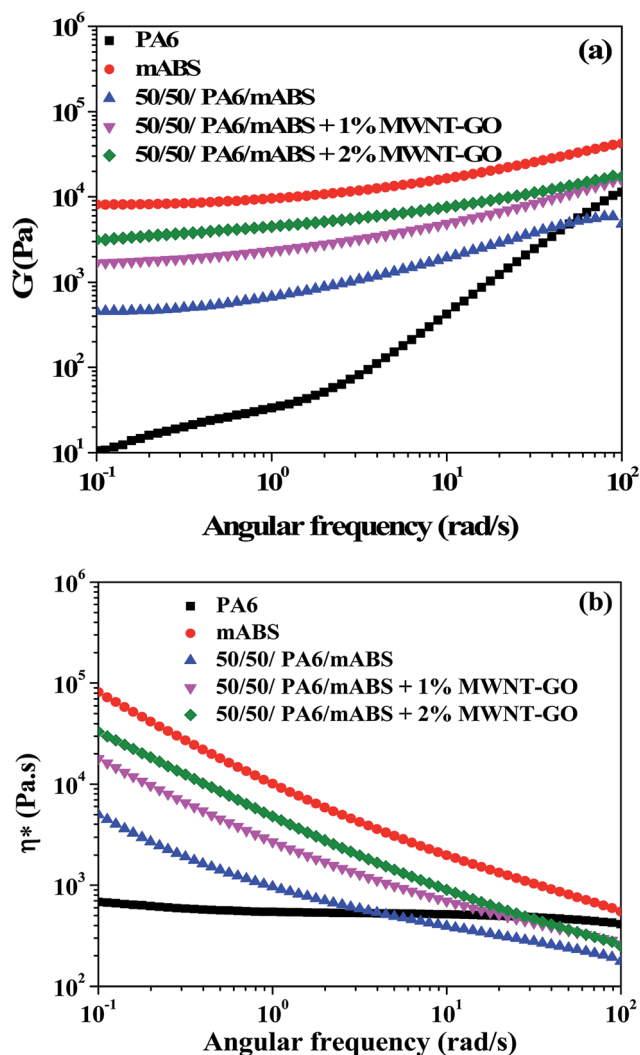Fig. 3 FT-IR spectra of mABS, PA6 and 50/50 PA6–mABS blend.

Fig. 4 Melt rheological properties: (a) storage modulus and (b) complex viscosity as a function of frequency for various blends and the constituent homopolymers.
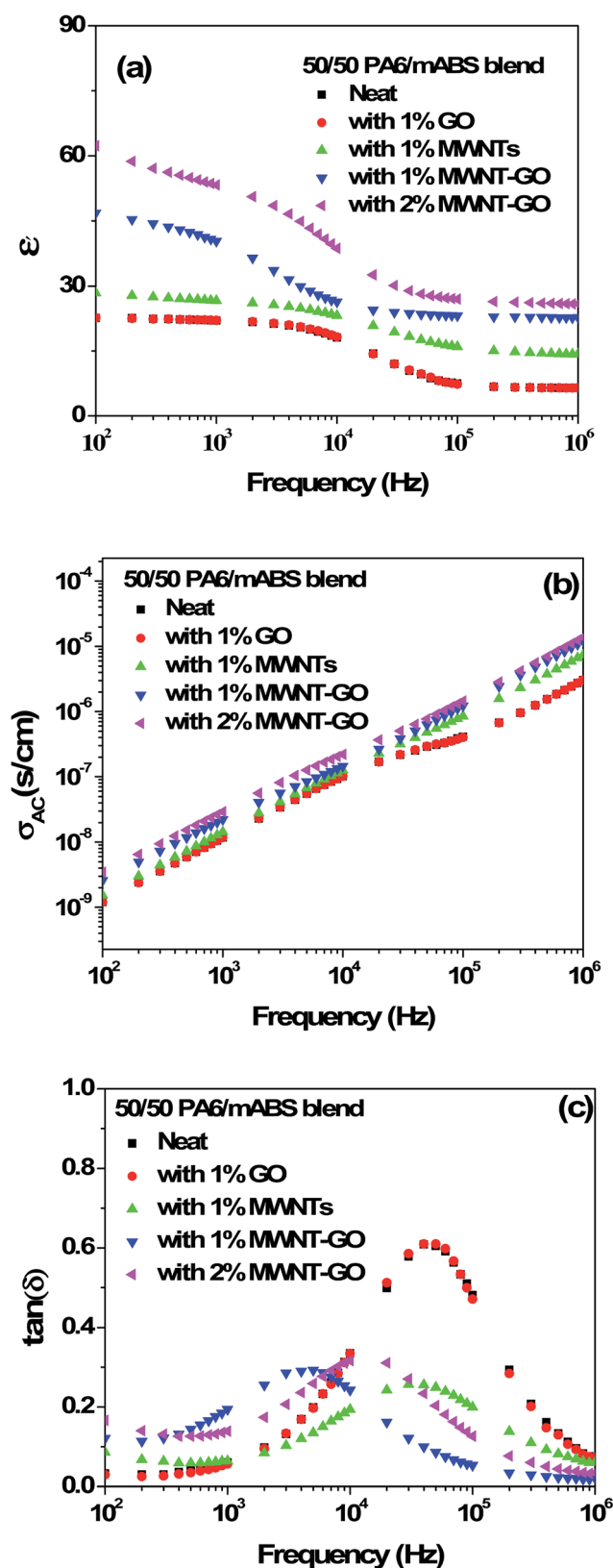
Fig. 5 (a) Dielectric constant, (b) AC electrical conductivity and (c) tan(δ) as function of frequency for various blends investigated here.

The complex viscosity of the blends as a function of frequency (Fig. 4b) clearly shows a pseudo-solid nature and distinct yield stress in the lower frequency region. Neat PA6 exhibited Newtonian like behavior in the measured frequency range, whereas mABS and the different blends showed a strong shear thinning behavior with yield stress in the lower frequency region.[25] The effect of particles on the flow properties is most prominent at lower frequencies where sufficient time is available for molecular relaxation. It was observed that the complex viscosity of the blends scaled with the fraction of MWNT–GO in the blends.[24]

Dielectric properties

Dielectric properties were measured at room temperature. Fig. 5a–c shows the dielectric constant (ε'), dielectric loss tangent (tan δ) and AC electrical conductivity (σ_{AC}) for the various blends investigated here. The dielectric constant of the blend substantially increased with respect to the neat blend upon addition of MWNT–GO hybrid nanoparticles. For instance, at 100 Hz, the neat blend showed a ε' of 22.5, whereas the blends with 1 wt% MWNT–GO and 2 wt% MWNT–GO showed a ε' of 46.5 and 62.5, respectively (Table 1). Interestingly, the hybrid MWNT–GO structures showed a higher dielectric constant compared to individual MWNTs (or GO). At 100 Hz the dielectric constants of the 50/50 PA6–mABS blend with 1 wt% GO and 1 wt% MWNTs were 22.5 and 28.5, respectively, and as explained above, the dielectric constant of MWNT–GO was much higher. The dielectric constant is increased by the easy polarization of the electrons residing in the π orbital of the MWNT–GO. The charge carrier originating under the electric field of the electrode migrates through the blend and accumulates at the interface as the relaxation time is different for the components. However, all the blends are insulating at room temperature (Fig. 5b). This is an ideal criterion for a dielectric material where the dielectric constant is higher but does not allow the free flow of electrons, thereby rendering insulating characteristics to the materials. This is also reflected in the dielectric loss tangent (Fig. 5c). The tan(δ) value of the neat blend is 0.02, and for the blends with MWNT–GO hybrid the loss tangent values are 0.12 (for 1 wt% MWNT–GO) and 0.16 (for 2 wt% MWNT–GO) at 100 Hz. So, the increase of the dielectric constant is attributed to the high interfacial polarization occurring at the interface of the blend and MWNT–GO.[11,33] The dielectric constant progressively increases with decreasing frequency. The components which are insulating, MWNTs which are conducting and GO sheets that are insulating but are composed of an abundant π-electron cloud, lead to a large disparity in the dielectric constant.[34] The increased dielectric

Table 1 Dielectric properties (at 100 Hz) of 50/50 PA6–mABS blends

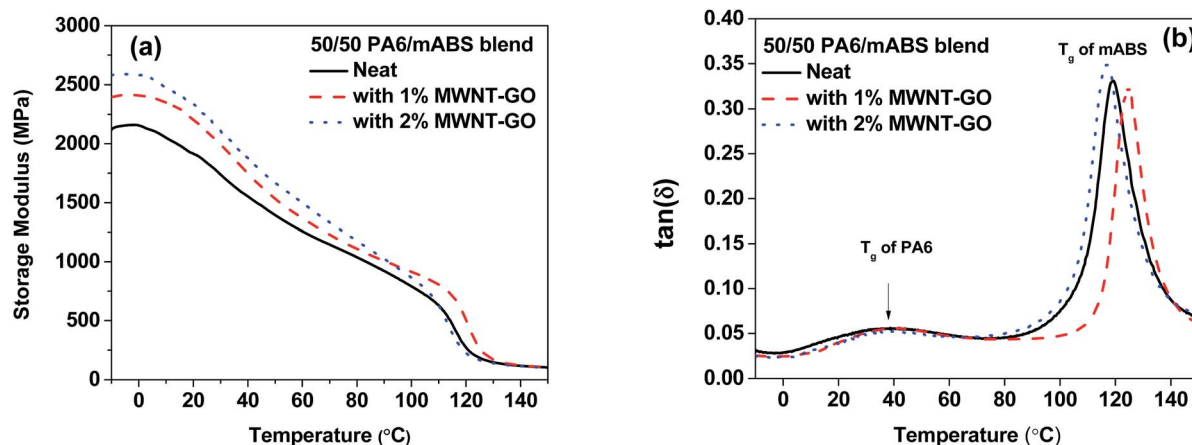| Blend	ε'	tan(δ)
50/50 PA6/mABS neat	22.5	0.02
50/50 PA6/mABS with 1 wt% GO	22.5	0.02
50/50 PA6/mABS with 1 wt% MWNT	28.5	0.08
50/50 PA6/mABS with 1 wt% MWNT–GO	46.5	0.12
50/50 PA6/mABS with 2 wt% MWNT–GO	62.5	0.16

Fig. 6 Dynamic mechanical thermal analysis for the various blends investigated here: (a) variation of storage modulus and (b) variation of tan(δ) with temperature.

dispersion seems to originate from the MWS effect (Maxwell–Wagner–Sillars polarization). This study clearly demonstrates that by anchoring MWNTs onto GO sheets, the dielectric constant of the material can be significantly enhanced, yet low dielectric loss achieved due to the restricted flow of electrons. It is a well-known fact that MWNTs enhance the dielectric constant of materials, however, also increase the dielectric loss due to leakage current. Hence, this unique strategy of anchoring MWNTs onto the GO sheets can trap charge at the interface of materials that show very different dielectric constants. Such materials can potentially be explored for capacitor applications.

Structural behaviour of the blends: effect of MWNT–GO

The reinforcing capability of the hybrid nanoparticles was evaluated by DMTA.[28] Fig. 6 shows the variation in elastic storage modulus (E') as a function of temperature. It is evident that in the lower temperature range (−10–100 °C) the storage E' is significantly higher for the blends with MWNT–GO, in striking contrast to the neat blends. It is evident from the melt rheological investigations that the hybrid nanoparticles form a pseudo-solid like structure in the blend. Hence, the increase in the elastic modulus can be related to the reinforcing effects of the hybrid nanoparticles. Moreover, the enhanced interfacial adhesion between the functional moieties on the GO sheets and PA6–mABS can facilitate better stress transfer at the interface. Interestingly, from the tan(δ) plots it can be observed that the T_g of mABS has decreased on addition of 2 wt% MWNT–GO, demonstrating the fact that the hybrid nanoparticles act as a plasticizing agent. The enhanced elastic storage modulus in the presence of MWNT–GO limits the possibility of chain scission. A more detailed investigation is required to get more insight in the plasticization effect in the presence of MWNT–GO hybrid particles.

Conclusions

In summary, a hybrid nanostructure of MWNTs anchored onto graphene oxide sheets was synthesized and melt blended with PA6–mABS blends. The hybrid nanoparticles were localized in

the PA6 phase of the blend as confirmed by electron microscopic techniques. The hybrid nanostructures enhanced the dielectric constant of the blends by three fold in striking contrast to the neat blends and interestingly, exhibited low dielectric loss. This enhancement was attributed to the increased specific surface area of the conductor–insulator hybrid particles leading to increased interfacial polarization in the blend. The elastic storage modulus also improved with the addition of MWNT–GO hybrid structures. Such materials can be explored for capacitor type applications.

Acknowledgements

References

1 K. Yang, X. Huang, L. Fang, J. He and P. Jiang, *Nanoscale*, 2014, **6**, 14740–14753.
2 C. Pecharromán, F. Esteban-Betegón, J. F. Bartolomé, S. López-Esteban and J. S. Moya, *Adv. Mater.*, 2001, **13**, 1541–1544.
3 Z. M. Dang, Y. H. Lin and C. W. Nan, *Adv. Mater.*, 2003, **15**, 1625–1629.
4 M. Sharma, S. Ranganatha, A. K. Kalyani, R. Ranjan, G. Madras and S. Bose, *Mater. Res. Express*, 2014, **1**, 045301.
5 J.-Y. Kim, T. Kim, J. W. Suk, H. Chou, J.-H. Jang, J. H. Lee, I. N. Kholmanov, D. Akinwande and R. S. Ruoff, *Small*, 2014, **10**, 3405–3411.
6 Q. M. Zhang, H. F. Li, M. Poh, F. Xia, Z. Y. Cheng, H. S. Xu and C. Huang, *Nature*, 2002, **419**, 284–287.
7 R. Liu, J. Wang, Q. Li, S. Li, S. Zhang and X. Ding, *J. Appl. Polym. Sci.*, 2014, **131**, DOI: 10.1002/app.39975.
8 L. Wang and Z.-M. Dang, *Appl. Phys. Lett.*, 2005, **87**, 042903.
9 C. Yang, Y. Lin and C. W. Nan, *Carbon*, 2009, **47**, 1096–1101.
10 J.-K. Yuan, S.-H. Yao, A. Sylvestre and J. Bai, *J. Phys. Chem. C*, 2011, **116**, 2051–2058.

11 P. Barber, S. Balasubramanian, Y. Anguchamy, S. Gong, A. Wibowo, H. Gao, H. J. Ploehn and H.-C. zur Loye, *Materials*, 2009, **2**, 1697–1733.

12 M. Arbatti, X. Shan and Z. Cheng, *Adv. Mater.*, 2007, **19**, 1369–1372.

13 D. K. Das-Gupta and K. Doughty, *Thin Solid Films*, 1988, **158**, 93–105.

14 P. Mishra and P. Kumar, *Compos. Sci. Technol.*, 2013, **88**, 26–32.

15 M.-F. Lin and P. S. Lee, *J. Mater. Chem. A*, 2013, **1**, 14455–14459.

16 L. Xie, X. Huang, C. Wu and P. Jiang, *J. Mater. Chem.*, 2011, **21**, 5897–5906.

17 S. Bose, R. A. Khare and P. Moldenaers, *Polymer*, 2010, **51**, 975–993.

18 C. Li, E. T. Thostenson and T.-W. Chou, *Compos. Sci. Technol.*, 2008, **68**, 1227–1249.

19 J.-Y. Kim, W. H. Lee, J. W. Suk, J. R. Potts, H. Chou, I. N. Kholmanov, R. D. Piner, J. Lee, D. Akinwande and R. S. Ruoff, *Adv. Mater.*, 2013, **25**, 2308–2313.

20 P. Xavier, K. Sharma, K. Elayaraja, K. S. Vasu, A. K. Sood and S. Bose, *RSC Adv.*, 2014, **4**, 12376–12387.

21 G. P. Kar, S. Biswas and S. Bose, *Phys. Chem. Chem. Phys.*, 2015, **17**, 1811–1821.

22 M. Kotal and A. K. Bhowmick, *J. Phys. Chem. C*, 2013, **117**, 25865–25875.

23 S. Bose, A. R. Bhattacharyya, P. V. Kodgire and A. Misra, *Polymer*, 2007, **48**, 356–362.

24 S. Bose, A. R. Bhattacharyya, A. P. Bondre, A. R. Kulkarni and P. Poetschke, *J. Polym. Sci., Part B: Polym. Phys.*, 2008, **46**, 1619–1631.

25 S. Bose, A. R. Bhattacharyya, A. R. Kulkarni and P. Pötschke, *Compos. Sci. Technol.*, 2009, **69**, 365–372.

26 S. Bose, A. R. Bhattacharyya, P. V. Kodgire, A. Misra and P. Pötschke, *J. Appl. Polym. Sci.*, 2007, **106**, 3394–3408.

27 L. Zhou, Y. Wan, X. Chen, S. Sun and C. Zhou, *Polym. Compos.*, 2014, **35**, 864–871.

28 S. Bose, A. R. Bhattacharyya, L. Häußler and P. Pötschke, *Polym. Eng. Sci.*, 2009, **49**, 1533–1543.

29 G. P. Kar, N. Begam, J. K. Basu and S. Bose, *Macromolecules*, 2014, **47**, 7525–7532.

30 G. P. Kar, P. Xavier and S. Bose, *Phys. Chem. Chem. Phys.*, 2014, **16**, 17811–17821.

31 G. P. Kar, A. Bharati, P. Xavier, G. Madras and S. Bose, *Phys. Chem. Chem. Phys.*, 2015, **17**, 868–877.

32 A. Bharati, P. Xavier, G. P. Kar, G. Madras and S. Bose, *J. Phys. Chem. B*, 2014, **118**, 2214–2225.

33 S. Y. Yang, K. Shin and C. E. Park, *Adv. Funct. Mater.*, 2005, **15**, 1806–1814.

34 J. W. Wang, Q. D. Shen, C. Z. Yang and Q. M. Zhang, *Macromolecules*, 2004, **37**, 2294–2298.